A Bayesian Network Approach for Condition Monitoring of High-Speed Railway Catenaries

Wang, Hongrui; Nunez, Alfredo; Liu, Zhigang; Zhang, Dongliang ; Dollevoet, Rolf

DOI
10.1109/TITS.2019.2934346

Publication date
2020

Document Version
Final published version

Published in
IEEE Transactions on Intelligent Transportation Systems

Citation (APA)
Wang, H., Nunez, A., Liu, Z., Zhang, D., & Dollevoet, R. (2020). A Bayesian Network Approach for Condition Monitoring of High-Speed Railway Catenaries. *IEEE Transactions on Intelligent Transportation Systems*, *21*(10), 4037-4051. Article 8805158. https://doi.org/10.1109/TITS.2019.2934346

A Bayesian Network Approach for Condition Monitoring of High-Speed Railway Catenaries

Hongrui Wang, *Student Member, IEEE*, Alfredo Núñez, *Senior Member, IEEE*, Zhigang Liu, *Senior Member, IEEE*, Dongliang Zhang, and Rolf Dollevoet

***Abstract*— The growing variety of data from condition monitoring of high-speed railways offer unprecedented opportunities to improve railway infrastructure maintenance. For condition monitoring of railway catenaries, this paper proposes a data-driven approach that uses a Bayesian network (BN) to integrate the inspection data from catenaries into a key performance indicator (KPI). The BN topology is structured based on the physical relationships among data types, including train speed, dynamic stagger and height of the contact wire, pantograph head acceleration, and pantograph-catenary contact force. The tailored performance indicators are individually defined and extracted from the five types of data as the BN input. As the output of the BN, the KPI is defined as the overall condition level of the catenary considering all defects that can be reflected by the data types. Finally, using historical inspection data and maintenance records from a section of the Beijing-Guangzhou high-speed line in China, the BN parameters are estimated to establish a probabilistic relationship between the input and output. An approach that applies the estimated BN to catenary condition monitoring is proposed. Testing of the BN-based approach using new inspection data shows that the output KPI can adequately represent the catenary condition, leading to a nearly 66.2% reduction in the false alarm rate of defect detection compared with current practice. It is also tested that when the input data quality is not ideal, the approach can still work acceptably on noisy data with a signal-to-noise ratio greater than 3 dB or with one type of data missing.**

***Index Terms*— High-speed railway, catenary, condition monitoring, Bayesian network, inspection data, key performance indicator.**

I. Introduction

CONDITION monitoring of the railway infrastructure currently plays an important role in railway asset management. It and enables condition-based maintenance that can improve the reliability, availability, and safety of the railway infrastructure. In recent years, emerging techniques have been developed for monitoring the conditions of the tracks [1]–[3], catenaries (overhead lines) [4]–[6], bridges [7], tunnels [8], etc. These techniques vary with the different demands of the railway networks, which are expanding worldwide [9].

The catenary is a predominant structure used in power transmission of electrified railways. It is normally constructed along the track with a contact wire suspended above so that trains can collect electric current from the catenary using a pantograph. Figure 1 shows the basic elements of a catenary and a pantograph mounted on the train roof. While a train is running on the track, the pantograph slides through and presses against the contact wire of the catenary, and thus electric current can flow from the contact wire to the train locomotive through the pantograph. To ensure that the trains have a continuous and stable power supply, it is important to maintain a good current collection quality resulting from the dynamic interaction between the catenary and pantograph [10]. Well-maintained catenaries not only enhance the safety and reliability of train operations but also lead to a reduction in life cycle costs. To this end, technical standards and specifications [11], [12] have been developed in which catenary condition monitoring is an indispensable measure. In China, defective catenaries require an average of more than 2 hours to repair, and up to 64% of these repairs lead to a loss of power for an average duration of 1.3 hours, which interrupts train services.

As a distributed structure spanning kilometers of distances, condition monitoring of the catenary is commonly performed by specialized inspection trains that run through the catenary such that the entire catenary structure can be covered. Traditionally, condition monitoring is periodically performed to inspect the geometrical parameters of the contact wire, including height, stagger and thickness [13], [14]. This approach is widely applied for conventional lines with an inspection interval between six months and one year. However, the geometrical parameters cannot reflect the dynamic response of the catenary in operation. Thus, dynamic parameters such as the contact force between the pantograph and catenary [4], [10], [15], the acceleration of the pantograph head (collector) [13], the displacement of the contact point [16], and the dynamic height and stagger of the contact wire [17], are

Manuscript received March 10, 2019; revised June 19, 2019; accepted August 7, 2019. Date of publication August 19, 2019; date of current version October 2, 2020. This work was supported in part by the National Natural Science Foundation of China under Grant U1734202, and in part by the Sichuan Province Youth Science and Technology Innovation Team under Grant 2016TD0012. The Associate Editor for this article was C. Guo. *(Corresponding author: Hongrui Wang.)*

H. Wang, A. Núñez, and R. Dollevoet are with the Section of Railway Engineering, Delft University of Technology, 2628 Delft, The Netherlands (e-mail: soul_wang0@163.com; a.a.nunezvicencio@tudelft.nl; r.p.b.j.dollevoet@tudelft.nl).

Z. Liu and D. Zhang are with the School of Electrical Engineering, Southwest Jiaotong University, Chengdu 610031, China (e-mail: liuzg_cd@126.com; zhangdongliang@my.swjtu.edu.cn).

Digital Object Identifier 10.1109/TITS.2019.2934346

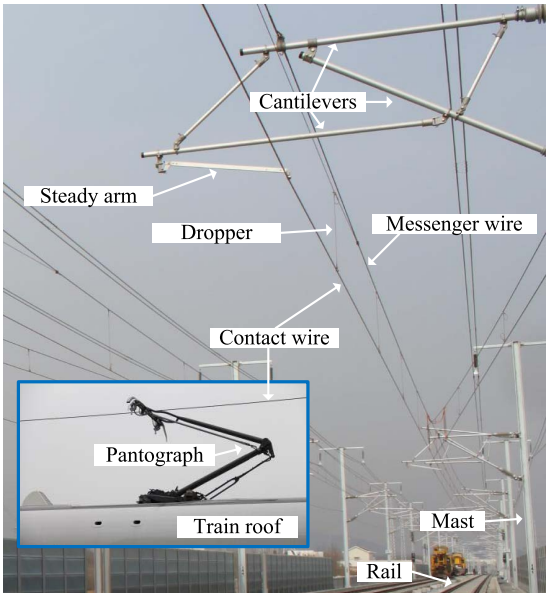

Fig. 1. Elements of a railway catenary and a pantograph.

becoming preferable in practice [18], [19], especially for high-speed lines. Other components of catenary systems, such as the insulator, isoelectric line, etc., are also monitored [20]–[22] because they are important to ensure the full functionality of the catenary.

Depending on the measurements applied for condition assessment, the condition of the catenary is commonly quantified by a performance indicator (PI) extracted from measurement data. For geometrical parameters, PIs consist mostly of comparisons with a threshold that is predefined according to nominal values or expert experience. The PIs based on dynamic parameters can be highly diverse because the dynamic responses of the catenary and pantograph, in terms of amplitude and frequency of vibrations, are contained in the measurement data. Therefore, the statistical distribution, kurtosis, power spectrum density and time-frequency representation of the pantograph-catenary contact force (PCCF) were selected as PIs to detect contact wire irregularities attributed to a wide range of catenary defects [10], [23]–[25]. As a substitute for PCCF, the pantograph head acceleration (PHA) is more cost-efficient to measure. Similarly, PIs such as the root mean square [13] and wavelet entropy [26] of the PHA were also chosen to detect contact wire irregularities. Based on the physical meanings of PIs, the condition of the catenary can be quantified for further assessment and maintenance decision-making.

In recent years, condition monitoring techniques deployed in practice are gradually making greater use of data-driven approaches [27]. For catenary condition monitoring, the types of geometrical and dynamic parameters measured and the increasing frequency of inspections [26] generates a large volume of multivariate data sets. However, approaches that can make full use of these data sets are lacking. In previous studies, PIs were mostly extracted from a single type of parameter. For defect detection of high-speed lines in China, the false alarm rate can reach up to 30.5% based on only one type of catenary data measured from a single inspection run, according to maintenance records. Learning from techniques developed for other applications, such as bearing fault diagnosis [28]–[30] and rail condition monitoring [31]–[33], improvements in condition monitoring of the high-speed railway catenary can be realized by the following:

1) Extraction of multiple PIs from one type of parameter;
2) Measurement of multiple parameters to extract and fuse the respective PIs.

This paper proposes an approach that combines both measures.

As specified in the technical standard for condition monitoring of high-speed railways in China [12], the PCCF, the PHA, and the dynamic height and stagger of the contact wire are simultaneously inspected by specialized measurement trains. Individually, these parameters can reflect the condition of the catenary under dynamic interaction with a pantograph, although from different perspectives, and they are also physically related to each other as the results of pantograph-catenary interaction. Because of the inherent physical relationships, the measurement data of the parameters contain probabilistic correlations in terms of dynamic responses. This feature can be used in enhanced condition monitoring in which the output rarely suffers from disadvantages due to a single type of data, such as measurement errors or missing data.

It is observed in the literature that multiple types of data are simultaneously measured and applied for monitoring the condition of a single system or device. For example, the diagnosis of power systems [34], airplane engines [35] and heat pumps [36] relies on multiple data types as the input. A similarity among these applications and catenary condition monitoring is fusion of multiple data types for assessment of the overall condition of a system. The data can be fused because of the probabilistic correlations between different data types indicating the healthiness of the same system. The Bayesian network (BN) [37], which mathematically represents a set of variables and their probabilistic relationships, can precisely address the data fusion problem described. Multiple PIs, each extracted from the different types of data measured for a catenary, can be fused using a BN to perform comprehensive condition assessment.

This study is an extension of a previous work [38]. In summary, the contributions and extensions of this study include the following:

1) A new BN is structured specifically for condition monitoring of the catenary.
2) Tailored PIs are proposed for different types of catenary inspection data and used as the input of the BN.
3) A data-driven approach using the BN is proposed to supply a comprehensive assessment of the catenary condition based on inspection data.

The remainder of this paper is organized as follows. Section II introduces the basic theory of BN. Section III proposes a BN for catenary condition assessment. Based on the proposed BN, an approach for catenary condition monitoring is presented in Section IV using inspection data from a high-speed railway line. Section V demonstrates the results

and performances of the approach. Conclusions are drawn in Section VI.

II. Bayesian Networks

BNs, also known as belief networks, are a type of probabilistic graphical model based on directed acyclic graphs [39]. This approach combines graph theory and probability theory, which makes it intuitively interpretable and mathematically rigorous. A BN constitutes of a set of random variables with conditional dependencies between the variables. In the directed acyclic graph of a BN, a node represents a random variable, and a directed arc pointing from node A (the parent node) to node B (the child node) indicates that the value of variable B depends on the value of variable A. Informally, the directed arc between a parent node and its child node forms a cause-effect relationship between the corresponding variables. This representation can be summarized as the local Markov property of BN, which states that each variable is independent of its nondescendents given its parent variables, where the descendants are the set of variables that can be reached on a direct path from the variable [40]. Although the directions of the arcs encode the cause-effect relationships among all variables, inference in a BN can be performed both forward along the arc directions and backward in the reverse directions. In practice, this feature enables estimation of the effect of an event when the status of causes is observed or identification of the causes when the effects are observed. This paper belongs to the former category.

A BN is defined by a pair (G, Θ), where G is a directed acyclic graph on a set of n nodes (variables) $\mathbf{X} = \{X_1, X_2, \ldots, X_n\}$ with independence assumptions among the variables according to the local Markov property, and Θ is a set of n conditional probability distributions $\Theta = \{p(x_1|\pi_1), \ldots, p(x_n|\pi_n)\}$ corresponding to each realization x_i of variable X_i conditioned on π_i, which is the set of parents of X_i in G. The joint probability distribution of variables $\mathbf{X}$ defined by the BN can be described as

$$p(\mathbf{X}) = \prod_{i=1}^{n} p(x_i|\pi_i). \tag{1}$$

When certain of the variables in the BN are observable, they supply evidence for the probabilistic inference of BN to obtain the posterior probability distributions of unobservable variables. This aspect is fundamental for BNs to address the uncertainties associated with diagnosis or prognosis [41], evaluation or assessment [42], forecast or prediction [43], etc.

For most practical problems, the BN must be learned from prior information and relevant data, including specification of both the graph structure and parameters of BN, to fully represent the joint probability distribution. Depending on the problem to be solved, the BN can be learned or estimated in the case in which the graph structure is unknown or certain variables are not fully observable. In this paper, the graph structure is first established based on the physical relationships among the variables involved in catenary condition monitoring. The parameters of the BN with the specific structure are estimated from historical measurement data. Because the overall condition of the catenary is considered to be a partially observable variable in the proposed BN, the BN parameters in such a case can be estimated by the expectation maximization algorithm [44] or the Markov chain Monte Carlo algorithm [45].

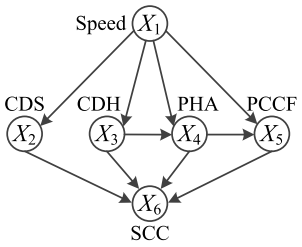

Fig. 2. Graph structure of the BN for catenary condition monitoring.

III. A BN for Catenary Condition Monitoring

A. Graph Structure

The directed acyclic graph G consists of $n = 6$ variables $\mathbf{X} = \{X_1, \ldots, X_6\}$ representing the speed of inspection train, the PIs extracted from the contact wire dynamic stagger (CDS) and dynamic height (CDH), PHA, PCCF, and the status of catenary condition (SCC), respectively. Figure 2 depicts the structure of graph G, where the conditional dependencies among the six variables are indicated by the directed arcs. The physical relationships underlying the structure are described as follows:

1) Variable X_1 represents the train speed at the moment when the data are measured. As a parent node, it is directed to the four variables representing the PI extracted from CDS, CDH, PHA and PCCF, respectively. This direction is based on the fact that the faster the train speed, the more intense the vibration excited between the pantograph and catenary, which leads to higher amplitude of oscillations in the four types of dynamic responses. Thus, the PIs from the four types of data are dependent on the level of train speed when the data are measured. At the same time, the speed of inspection train itself is irrelevant to the SCC, and thus no arc is connecting the two variables.

2) Variables X_2, X_3, X_4, and X_5 represent PIs extracted from CDS, CDH, PHA and PCCF, respectively. Because they are all indicators for the SCC X_6, they affect the value of the SCC with four directed arcs pointing to the SCC in the graph structure shown in Figure 2.

3) Variable X_2 represents the PI extracted from the CDS, which is the only parameter measured in the lateral direction parallel to the ground. This variable reflects whether the stagger of the contact wire is within an acceptable range for pantograph contact. The CDS is not physically related to the data of CDH, PHA and PCCF, because the latter three parameters are defined and measured in the direction vertical to the ground.

4) Variables X_3, X_4, and X_5 represent the PIs extracted from CDH, PHA and PCCF, which are all dynamic responses in the vertical direction. Assuming that at a time instant t during the pantograph-catenary interaction, the CDH $h_c(t)$ is uplifted

by the pantograph head with an acceleration $a_p(t)$. If the contact between the pantograph and catenary is continuously maintained by the PCCF $f_c(t) > 0$, the CDH $h_c(t)$ becomes numerically equivalent to the vertical displacement of the contact point, and the PHA $a_p(t)$ becomes equivalent to the vertical acceleration of the contact point. Thus, the relationship between the CDH $h_c(t)$ and the PHA $a_p(t)$ can be written as

$$a_p(t) = \frac{d^2}{dt^2} h_c(t). \tag{2}$$

This relationship can be transformed from the time domain to the frequency domain by the Fourier transform as

$$\widehat{a_p}(\xi) = \mathcal{F}\left(a_p(t)\right) = (2\pi i\xi)^2 \widehat{h_c}(\xi) = -4\pi^2 \xi^2 \widehat{h_c}(\xi) \tag{3}$$

where $\mathcal{F}\left(a_p(t)\right)$ denotes the Fourier transform of $a_p(t)$, $\widehat{h_c}(\xi) = \mathcal{F}\left(h_c(t)\right)$, and ξ denotes frequency. This formulation reflects that

$$\left|a_p(\xi)\right| \propto \left|\xi^2 \widehat{h_c}(\xi)\right|. \tag{4}$$

Therefore, when the vibration response induced by a defect or fault of the catenary with a certain frequency can be captured by the CDH, it can also be observed from the PHA with a higher level of spectral energy. This representation forms a correlation between the PIs of CDH and PHA that can be mapped into the directed acyclic graph of BN as a directed arc between the two variables, as shown in Figure 2. In the measurements, the PCCF $f_c(t)$ is considered to be the sum of three component forces [46], [47], i.e. the pressure measured by force sensors $f_{\text{sensor}}(t)$, the inertia force $f_{\text{inertia}}(t)$ and the correction of aerodynamic force $f_{\text{aero}}(t)$,

$$f_c(t) = f_{\text{sensor}}(t) + f_{\text{inertia}}(t) + f_{\text{aero}}(t). \tag{5}$$

The inertia force $f_{\text{inertia}}(t)$ is calculated depending on where the force sensors are installed on the pantograph. If the sensors are installed under the pantograph head, i.e., the majority of the cases, the inertia force is given by

$$f_{\text{inertia}}(t) = m_p \cdot a_p(t) \tag{6}$$

where m_p is the mass of the pantograph head. It can be observed that the measurement data of PCCF depend on the PHA data. The PCCF $f_c(t)$ inherits a portion of the dynamic responses contained in the PHA $a_p(t)$. Thus, a directed arc pointing from variable X_4 to variable X_5 is established in the BN, as shown in Figure 2, indicating a cause-effect relationship between the data of PHA and PCCF.

Through the relationships formed between the six variables, the graph structure of the BN supplies a physics-based model that integrates all available sources of PIs to comprehensively evaluate the SCC. The next step is quantifying the SCC, namely, obtaining a comprehensive key performance indicator (KPI) of the catenary by specifying the probabilistic relationships between the variables based on historical observations.

B. Variable Extraction

The observations of the six variables are extracted from historical measurement data, and the method of extraction varies for each variable. As a prerequisite, the different types of measurement data should be synchronized to ensure matching sampling frequency and spatial location. A synchronized data set ensures that the data of different catenary parameters reflect the same dynamic responses excited at the same moment. This condition is fairly important for obtaining accurate probabilistic relationships between variables. In practice, it is uncommon to have perfectly synchronized data because the data are measured by separate sensors, especially when the inspection train runs at a high speed. Therefore, it is necessary to mitigate synchronization errors that might cause inaccurate outputs generated from the data. This synchronization can be performed by calibrating the position of all data based on a unified reference position in the data set. In addition, the data can also be reconstructed by downsampling to a lower frequency to offset minor errors in position. In this manner, synchronization errors between different data types can be mitigated, especially those leading to shifting of features in spatial position.

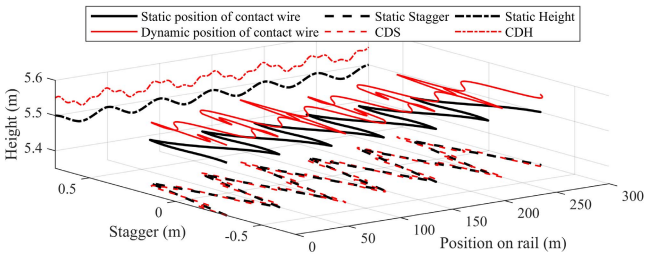

Fig. 3. Comparison between the static and the dynamic spatial position of contact wire.

The following describes the PI extraction of every variable in a manner that best reflects and quantifies the catenary condition.

1) Speed X_1: As the only variable with unconditional probability in the proposed BN, the train speed X_1 is of great importance. Without knowing the level of train speed, evaluation of the catenary condition based only on the four types of dynamic responses is meaningless and invalid. To establish a corresponding relationship between the level of speed and the intensity of the dynamic responses using the available data, a step size s_{step} is chosen to partition the data into different levels of speed. This step size is selected to ensure that sufficient data are measured under each level of speed for estimation of the parameters of BN. In this way, the data for extracting variables X_2, X_3, X_4 and X_5 are automatically partitioned by the levels of speed.

2) CDS X_2 and CDH X_3: Compared with the static position of the contact wire, the dynamic position of the contact point during operation (hereafter referred as the dynamic position of the contact wire) vibrates in both the vertical and lateral directions, resulting in the CDS and CDH, as schematically shown in Figure 3. For evaluation of the catenary condition, the CDS and CDH behave in a similar manner and are normally equal to or greater than the static values because a positive contact force always uplifts and also laterally deflects the contact wire. Thus, an excessive peak or trough in the

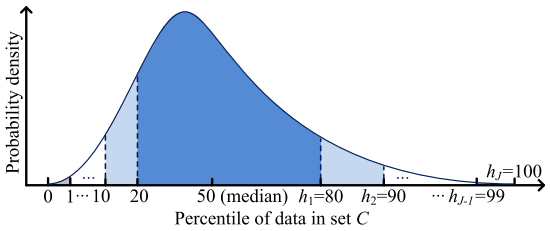

Fig. 4. Illustration of the percentile-based clustering.

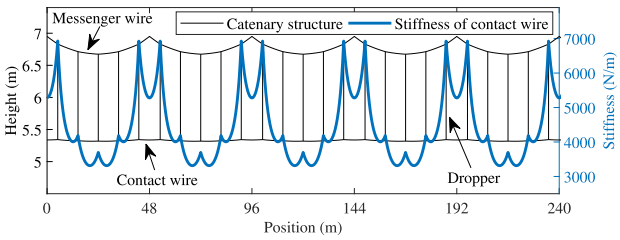

Fig. 5. Schematic of contact wire stiffness varying cyclically with the catenary structure. The left vertical axis shows the height of catenary structure including the messenger wire, contact wire and droppers, and the right vertical axis shows the stiffness.

CDS and CDH indicates a strong impact on the contact wire, loss of contact, or abnormal contact wire positioning, which reflects an unfavorable condition that requires attention.

To extract PIs for variables CDS X_2 and CDH X_3 that can supply evidence for variable X_6, the frequency contents contained in the CDH and CDS are not extracted because according to (4), an anomaly is more significantly perceived in the frequency domain of acceleration rather than that of displacement. Additionally, in the proposed BN, the frequency-domain PI is considered for variable X_4. Therefore, the PIs for variables X_2 and X_3, both extracted from a measure of displacement, are time-domain indicators determined by the deviations of CDS and CDH from their healthy states. The definitions of healthy states for CDS and CDH are dependent on the levels of speed segmented by the step size s_{step}. Based on large amounts of historical data partitioned into every speed level, the PIs of CDS X_2 and CDH X_3 can be extracted at each speed level, thus building the dependencies of X_2 and X_3 on the speed level X_1.

To determine whether the value of CDS or CDH is healthy or not, the judgement is highly dependent on the monitored catenary because the structural parameters (including the suspension type, nominal position of contact wire, contact wire tension, etc.) are diverse by design for different railway lines. Thus, the healthy range of variation for CDS and CDH should be defined with respect to the change in speed for a specific catenary. This definition can be constructed in a data-driven manner based on sufficient historical data from the same catenary. It is also implied that the majority of the observations should represent a healthy condition of the catenary for the data to be sufficient. The percentile of available observations can be used to perform statistics-based clustering in which the probability of a value falling into a certain condition level is quantitatively considered.

Concretely, assuming that a set of CDS or CDH data $C = \{c_1, c_2, \ldots, c_N\}$ is partitioned to a certain speed level, the N observations can be clustered into J $(2 \le J \le N)$ sets $\mathbf{S} = \{S_1, S_2, \ldots, S_J\}$ corresponding to J levels of condition of CDS or CDH, which are viewed as the time-domain PIs extracted from CDS or CDH at the specific speed level. As an example shown in Figure 4, the observations in C can be clustered based on the percentile intervals defined by the percentile boundary of healthy observations h_1, which is defined as the data located in the middle of the full percentile, and the percentile boundaries of unhealthy observations $\{h_2, \ldots, h_J\}$, which are data located at both ends of the full percentile. This representation can be mathematically written as

$$S_j = \begin{cases} P(h_1) \setminus P(100 - h_1), & j = 1 \\ P(h_j) \setminus P(100 - h_1) \setminus \bigcup_{m=1}^{j-1} S_m, & 2 \le j < J \\ P(100) \setminus \bigcup_{m=1}^{J-1} S_m, & j = J \end{cases} \tag{7}$$

where '\' denotes the set difference operator, and $P(h_j)$ denotes the h_jth percentile of the data in set C. To include all data in C, h_J should be equal to 100. The selection of $h_1 (h_1 > 50)$ determines the tolerance of the system against unhealthy conditions reflected by CDS or CDH, and the sensitivity to report such unhealthy conditions through the system. The number of levels J depends on the demand to subdivide the levels of unhealthy conditions; nevertheless, it cannot be too large by displaying too many levels of unhealthy conditions that produce redundant information. Normally, a classic description of healthy or low, medium, high or extreme risk levels in risk assessment can be sufficient, meaning that $J = 5$. In this context, the values from h_2 to h_J should ascend in a decelerating manner such that S_J contains the smallest set of data for the most extreme condition. When the CDS or CDH data partitioned to every speed level are clustered based on the corresponding percentiles, the influences of speed on CDS or CDH are automatically considered for evaluation of the catenary condition.

3) PHA X_4 and PCCF X_5: As noted by previous studies [24], [26], both PHA and PCCF contain frequency contents that are useful for reflecting the catenary condition. In particular, the catenary structure wavelengths (CSWs) have a strong correlation with the catenary structure, including anomalies such as installation errors and structural defects. As shown in Figure 5, the CSWs are frequency components of PHA and PCCF attributed to the cyclic variation of the contact wire stiffness along the catenary structure. Thus, the PHA and PCCF can be decomposed into two signals, namely, the CSWs and the non-CSW signal. The former is often used as an indication for structure-related defects, and the latter mostly reflects local defects such as hard points and uneven wear on the contact wire. In this way, diagnoses based on PHA and PCCF can be performed with less interference and thus output more accurate results compared with the situation in which the PHA and PCCF are not decomposed. Empirical mode decomposition (EMD) [48] is commonly selected to

perform an adaptive decomposition so that the PHA and PCCF measured from different catenary systems can be consistently decomposed into the CSWs and the non-CSW signal. The general steps needed to obtain the two signals are described as follows using the PCCF signal $f_c(t)$ as an example:

Step 1: Decompose the PCCF signal $f_c(t)$ into a number of intrinsic mode functions (IMFs) $f_{c,l}(t)$ and a residual $r(t)$ using EMD or its improvements,

$$f_c(t) = \sum f_{c,l}(t) + r(t). \tag{8}$$

Step 2: Identify the CSWs from all IMFs by checking whether the dominant wavelength (or spatial frequency) of an IMF falls into the range of structure wavelengths. Two generic wavelength intervals [4m,10m] and [40m,70m] indicating the wavelengths of interdropper distances and spans, respectively, can be used in the identification, even if no prior information on the catenary is available to narrow them down.

Step 3: Based on the IMFs identified as CSWs $f_{c,l}(t)$, $l \in C$, compute the CSWs $f_{c,C}(t)$ and non-CSW signal $f_{c,N}(t)$ by

$$f_{c,C}(t) = \sum_{l \in C} f_{c,l}(t) \tag{9}$$

and

$$f_{c,N}(t) = \sum f_{c,l}(t) - f_{c,C}(t), \tag{10}$$

respectively.

After obtaining the CSWs and the non-CSW signal of PHA and PCCF, the energy density of both signals corresponding to the instantaneous frequencies can be computed as the sources of frequency-domain PIs. Using the CSWs of PCCF $f_{c,C}(t)$ as an example, the analytic forms of its IMFs $f_{c,l}(t)$, $l \in C$ can be obtained with the Hilbert transform:

$$z(t) = f_{c,l}(t) + i \cdot \mathcal{H}[f_{c,l}(t)] = a(t)e^{i\theta(t)} \tag{11}$$

where $\mathcal{H}[f_{c,l}(t)]$ denotes the Hilbert transform of $f_{c,l}(t)$,

$$a(t) = \sqrt{f_{c,l}(t)^2 + \mathcal{H}[f_{c,l}(t)]^2} \tag{12}$$

and

$$\theta(t) = \arctan\left(\frac{H[f_{c,l}(t)]}{f_{c,l}(t)}\right). \tag{13}$$

The instantaneous frequency is defined as

$$\omega(t) = \frac{d\theta(t)}{dt}. \tag{14}$$

Thus, the Hilbert spectrum of $f_{c,C}(t)$ can be obtained as the real part $\mathcal{R}$ in the following form

$$H(\omega, t) = \mathcal{R}\left\{\sum_{l \in C} a(t) \exp\left[i \int \omega(t) dt\right]\right\} \tag{15}$$

which is a time-frequency representation showing the energy density distributed with the change in time and instantaneous frequency. To examine the instantaneous energy level of the CSWs $f_{c,C}(t)$ at a certain time instant, the accumulated energy density can be computed as

$$A(t) = \sum_{l \in C} a(t)^2. \tag{16}$$

This parameter indicates the intensity of vibration at a frequency range identical to that of the CSWs or non-CSW signal. It can thus be applied for fault diagnosis in general and also supplies PIs for the catenary at the specific location.

The PIs input into the BN as values of variable PHA X_4 and PCCF X_5, similar to the time-domain PIs extracted from CDS and CDH, should be indicators clustered into different levels. For consistency with the PIs from CDS and CDH, it is ideal that those from PHA and PCCF share the same number of condition levels. Because the PIs result from the same excitations, a certain coherence is preserved if they are clustered in the same way, in the sense that an equivalent PI among the four types of variables indicates the same degree of 'unhealthiness' or defect. Moreover, this coherence can be passed down to the final variable SCC X_6 in the form of evidence for probabilistic inference. However, both PHA and PCCF are decomposed into two signals and thus have two independent indicators $A_C(t)$ and $A_N(t)$ via (16) from the CSWs and the non-CSW signal, respectively. Both indicators represent the catenary condition in the frequency range corresponding to their own physical meanings. This is a unique feature of the indicators extracted from PHA and PCCF, because no such frequency contents can be found in CDS and CDH. Thus, a PI of variable X_4 or X_5 should be constructed to preserve the information contained in both indicators. A maximum criterion is proposed to combine the two indicators. Concretely, for the PHA or PCCF, indicators $A_C(t)$ and $A_N(t)$ can be partitioned by the same speed levels defined by step s_{step} such that the influences of speed variation are eliminated. Sets C_C and C_N are indicators partitioned to a same speed level from $A_C(t)$ and $A_N(t)$, respectively. Using percentile-based clustering according to (7), sets $\mathbf{S}_C = \{S_{C,1}, S_{C,2}, \ldots, S_{C,J}\}$ and $\mathbf{S}_N = \{S_{N,1}, S_{N,2}, \ldots, S_{N,J}\}$ can be obtained from C_C and C_N, respectively. Consequently, this formulation gives a condition level to every value in $A_C(t)$ and $A_N(t)$. Assuming at any time instant t',

$$A_C(t') \in S_{C,a} \text{ and } A_N(t') \in S_{N,b}. \tag{17}$$

which equivalently assigns condition levels, namely, PIs a and b to $A_C(t')$ and $A_N(t')$ as

$$L_C(t') = a \text{ and } L_N(t') = b. \tag{18}$$

The maximum criterion defines a combined PI as

$$L(t') = \max(L_C(t'), L_N(t')). \tag{19}$$

In this manner, an unhealthy condition can be always reported regardless of its indicative frequency range. It is not only consistent with PIs of CDS and CDH, but also offers necessary evidence for the variable SCC X_6.

TABLE I
LIST OF SCC VALUES (KPIS) WITH RESPECT TO VERIFYING PARAMETERS

#	Verifying parameter	# of severity levels	SCC X_6
1	Contact wire height	4	[1,5]
2	Height difference in a span	2	{1,3,5}
3	Contact wire stagger	4	[1,5]
4	Maximum PCCF	4	[1,5]
5	Minimum PCCF	4	[1,5]
6	Standard deviation PCCF	2	{1,3,5}
7	Hard point	4	[1,5]
8	Duration of arcing	2	{1,3,5}
9	Percentage of arcing	2	{1,3,5}
10	Angle of steady arm	1	{1,3}
11	Catenary voltage	1	{1,3}
12	EMU current	1	{1,3}

4) SCC X_6: This is the only variable with partial observability in the BN and is also an output as the quantification of SCC for maintenance decision-making. In this context, the available observations of variable X_6 are defined as the severity of defects that are detected in an inspection run and, most importantly, verified later by human inspectors on site. Due to the massive workload required to perform manual verifications, in most cases, only a portion of historical inspection results can be selectively verified and recorded as observations, thus creating the partial observability.

Although the protocols established to verify catenary defects differ from one railway line to another, the results normally conclude whether a defect exists and its severity. The SCC X_6 supplies such a conclusion based on the evidence given by the other variables, whereas previously, only the observations from one variable in a single run were considered. Thus, the value of SCC is the overall condition level of the catenary, namely, a KPI that considers all potential defects reflected by the available observations of other variables. This can be achieved by unifying the different severities of all known defect types. Based on expert experience, the unified value can be manually estimated according to the severity of defects defined in protocols. In a protocol designed to quantify the severity level of catenary defects, the severity levels are commonly defined by a group of multidisciplinary experts who consider both the mechanical and electrical performances of the catenary. To propose a unified severity level considering all types of defects, the potential negative effects or consequences of a defect at different severity levels should first be quantitatively estimated in terms of cost, loss of time, etc. Subsequently, the probability of such effect actually occurring is also estimated using maintenance records and available knowledge. By multiplying the effect with the corresponding probability, the risk of a defect can be obtained as a unified value indicating the healthiness of the catenary. In this manner, a unified condition level can be defined rationally with controllable variations depending on the accuracy of the effect and probability estimations.

As a new paradigm, Table I proposes a summarized list of the estimated catenary condition levels in the case of high-speed lines in China. The condition levels correspond to a certain type of catenary defect indicated by a verification parameter measured on-site. A total number of 12 verification parameters, each with several levels of severity determined by predefined thresholds, are assigned to the unified values of SCC X_6 as a standardization effort. It can be observed from Table I that depending on the type of verification parameter, the numbers of the severity levels are different. This scenario is defined by the protocol for inspection of high-speed railway catenaries, in which parameters such as the contact wire height are divided into four levels of value corresponding to four severity levels, and other parameters such as the percentage of arcing has two levels and the catenary voltage has one level, meaning that it is out of a required range. The values of SCC, namely, the KPIs range from 1 to 5 with 1 representing a healthy state and higher values representing unhealthier conditions. The range is consistent with the values defined for variables from X_2 to X_5. This list is applied to obtain the available observations of variable X_6 that indicate the verified condition level of the catenary in the maintenance record. In addition, a number of observations with value 1 (healthy) are assigned to variable X_6, when the corresponding observations of variables from X_2 to X_5 are 1, showing no indication that the catenary is unhealthy. Similarly, a number of observations with value 5 (extreme risk) are also assigned when the observations of the four variables are all equal to 5. For a specific railway line, the list can be modified by considering the differences in operation condition and pantograph-catenary dynamic characteristics.

C. Parameter Estimation

The proposed BN has a known structure but incomplete observability for variable SCC X_6. In the case of full observability, the maximum likelihood estimation can directly find a set of parameters that maximize the likelihood function of the given set of probabilistic relationships defined by the BN structure. When data are partially missing, an initial set of BN parameters can be assumed to complete the missing data through inference. A new expected likelihood function can be computed based on the newly completed data set. This procedure is known as expectation. The set of BN parameters can be updated by maximizing the current expected likelihood function, which is known as maximization. By iterating between the expectation and the maximization, a final set of parameters can be eventually estimated when the likelihood function converges, which is the well-proven realization of the expectation maximization (EM) algorithm for estimating parameters of the BN with incomplete data [44]. The use of the EM algorithm requires that the data are missing at random, meaning that the value of X_6 and the event that X_6 is missing are conditionally independent, given other observed variables, which is true in this case because the existence of SCC is independent of whether the SCC is verified on site or not.

In this application, the parameters estimated based on a set of data by nature inherit the dynamic characteristics of the specific catenary type and pantograph-catenary couple from the line on which the data set is measured. Therefore, the input data should be measured from the same railway line when the same pantograph is mounted. This situation is often realized by a specialized inspection train.

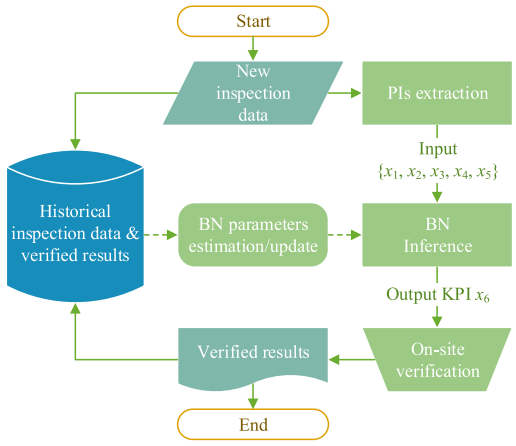

Fig. 6. Brief flowchart of the BN-based approach. The dashed lines denote alternative flows.

IV. A BN-Based Approach

Based on an established BN, a data-driven approach for catenary condition monitoring is proposed. Figure 6 depicts the general architecture of the approach for a railway line with inspection data available. The approach initiates with BN parameter estimation. New inspection data can subsequently be input for catenary condition assessment. The BN parameters are updated after on-site verifications are performed.

When the BN parameters are estimated, the ratio of variation (ROV) of a parent variable to its child can be computed. This value quantifies the importance or contribution of a parent variable that leads to the value of its child. For the proposed BN, the ROV can be used to describe which of the four variables representing the PIs of CDS, CDH, PHA and PCCF, respectively, have more impact on the final KPI of SCC. Concretely, the ROV of variable X_i with respect to the final variable X_6 is defined as:

$$R(X_i) = \frac{p(x_i \neq 1 | x_6 = j) - p(x_i \neq 1)}{p(x_i \neq 1)} \tag{20}$$

where $p(x_i \neq 1)$ is the marginal probability of $x_i \neq 1$, representing the probability that variable X_i is unhealthy.

A. Input

An estimated BN can be applied as a diagnostic tool formulated based on the historical data for parameter estimation and expert knowledge for defect verification and severity quantification. Because the BN is estimated using inspection data from a certain railway line, it can only function correctly when the input is also extracted from new data measured in the same line. New inspection data containing CDS, CDH, PHA and PCCF together with the train speed can be used in input extraction. The BN inputs are values of variables from X_1 to X_5, namely, the speed level, PIs extracted from CDS, CDH, PHA and PCCF. The PIs should be extracted in the same manner as described in the previous section and summarized as follows:

Step 1: Synchronize data with respect to sampling frequency and spatial position.

Step 2: Decompose the PHA and PCCF data into CSWs and non-CSW signal by (9) and (10).

Step 3: Partition the CDS, CDH, decomposed PHA and PCCF data into different speed levels determined by a step size s_{step}.

Step 4: Extract the PIs of CDS and CDH based on their data percentiles using (7), and the PIs of PHA and PCCF using (19).

It should be noted that the BN parameters can always be updated by new inspection data and the corresponding verified defects. This update can be performed regularly to make the BN more knowledgeable and up to date for catenary condition assessment. The feedback loop formed among the BN-based condition assessment, the on-site defect verification and the BN parameter updates can further improve the accuracy of condition assessment and defect detection.

B. Output

Given the BN input, i.e., the values of variables from X_1 to X_5, as evidence for BN inference, the posterior probability of the final KPI $x_6 = j$, i.e., $p(x_6 = j | \{x_2, x_3, x_4, x_5\})$, can be inferred. The expectation of the posterior probability distribution of variable SCC X_6 can be computed as the final output:

$$E(X_6) = \sum_{j=1}^{J} p\left(x_6 = j | \{x_2, x_3, x_4, x_5\}\right) \cdot j. \tag{21}$$

The output KPI indicates the expected condition level of the catenary at the corresponding location where the data are measured. Alternatively, the output KPI can be the most probable value of variable X_6

$$\arg\max_j p\left(x_6 = j | \{x_2, x_3, x_4, x_5\}\right). \tag{22}$$

This KPI of SCC is stricter and especially useful for recognizing unhealthy conditions compared with the expected value. Depending on the preference of the decision makers, the expected value can be used in general condition assessment, and the most probable value is better for determining whether a track visit is necessary by looking at SCC at suspicious unhealthy locations.

V. Results and Performance Discussions

This section presents the results of BN estimation and application of the estimated BN. The condition monitoring performances of the BN-based approach for reducing false alarms and addressing low-quality data are discussed. Hereafter, the potential defects of the catenary represent defects that are identified based only on the inspection data without on-site verifications. When on-site verifications are performed for the potential defects, the hits and false alarms are defined as the successfully verified defects and falsely identified defects, respectively. Accordingly, the hit rate and false alarm rate are the ratios of the numbers of hits and false alarms to the total number of potential defects, respectively. In practice, because on-site verifications were not performed for every

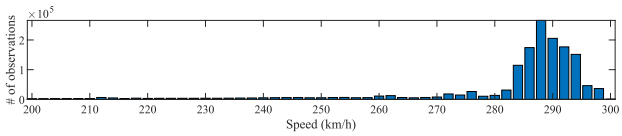

Fig. 7. Number of observations distributed with inspection train speed.

potential defects found from historical data, this study considers the defects that were actually verified when calculating the number hits and false alarms detected by the proposed approach.

A. BN Estimation

The BN parameters can be estimated through available observations extracted from historical data. In this paper, the data used as the source of observations are periodic inspection data measured from a section of Beijing-Guangzhou high-speed line in China during a period from December 2014 to June 2018. All measurements of speed, PCCF, PHA, CDH and CDS have a synchronous sampling interval of 0.25 m with the position recorded and calibrated by differential GPS and radio-frequency identification (RFID) using RFID tags attached on the masts of the catenary along the railway line. Observations of variables are extracted per procedures presented in the previous section. As a result of the periodic inspection, approximately 1.546×10^6 observations are acquired from an accumulated mileage of 1546.4 km of the catenary in the same section of railway line with the speed of the inspection train ranging from 100kmh^{-1} to 300kmh^{-1}. Data measured below 100kmh^{-1} are omitted because the data size is too small to represent a set of balanced observations at lower speed levels. These data can still be added for estimation of the BN parameters if sufficiently collected. Figure 7 shows the number distribution of observations with respect to the speed above 200kmh^{-1}, which contains 94.9% of all observations. Because the inspection train is dedicated to run near 290kmh^{-1} in every inspection, 78.7% of observations are located at speeds between 280kmh^{-1} and 300kmh^{-1}. Other speeds are mostly measured when the inspection train is accelerating or decelerating.

In this study, the step size s_{step} =2kmh^{-1} is selected for data partitioning, meaning that for every 2kmh^{-1} increase from zero speed, the data measured within an increment are considered under the same speed level. Once all data are partitioned by speed levels X_1, the values of variables from X_2 to X_5 are extracted. Figure 8 depicts the PI values j of CDS X_2 and CDH X_3 clustered by (7) using the set of percentile boundaries $\{h_1, \ldots, h_5\} = \{95, 97.5, 99, 99.8, 100\}$, which represent the condition level of healthy, low risk, medium risk, high risk, and extreme risk, respectively. It can be generally observed that the greater the speed, the larger the deviation of CDS and CDH. An outburst of extreme-risk conditions occurs at approximately 290kmh^{-1}, because the observations are concentrated at this speed level, which is close to the highest speed designed for this railway line. The clustered CDS in Figure 8(a) are evenly distributed around the median, which is approximately zero, whereas the median of CDH and

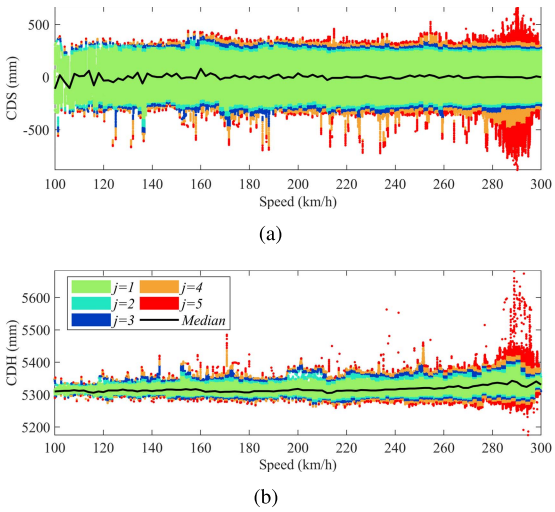

Fig. 8. Clustered (a) CDS and (b) CDH with respect to speed levels.

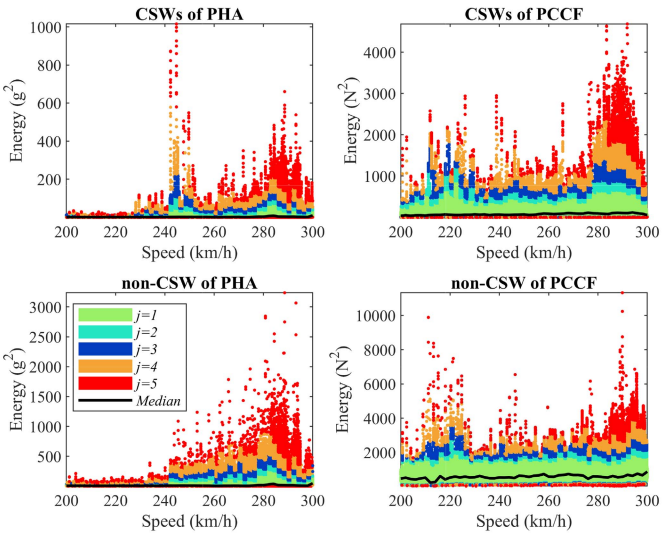

Fig. 9. Clustered instantaneous energy of CSWs and non-CSW signal of PHA (left) and PCCF (right).

the range of healthy CDH ($j = 1$) gradually increase as the speed increases in Figure 8(b). A sudden narrowing of the CDH range can be noted near the highest speed level, which is caused by the drastic drop in observation number starting from 296kmh^{-1}, as shown in Figure 7.

For variables X_4 and X_5, the CSWs and non-CSW signal are first extracted to obtain the accumulated instantaneous energy via (16). Using the same percentile boundaries for CDS and CDH, Figure 9 depicts the clustered energy of the CSWs and non-CSW signal of PHA on the left and those of PCCF on the right. It can be observed that the distribution of unhealthy indicators ($j > 1$) differs between the CSWs and the non-CSW signal, and between the PHA and PCCF. In all four types of clustering results, the catenary condition worsens at high speeds near 290kmh^{-1}. On the left, the CSWS of PHA reveals a particularly sensitive speed at approximately 245kmh^{-1}, where the condition also worsens, whereas the result of non-CSW signal shows no such particularity. This

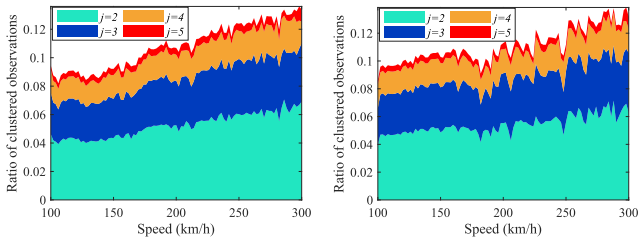

Fig. 10. Clustering results from (a) PHA and (b) PCCF showing the ratio of clustered observation number to the total observation number at every speed level when $j \geq 2$.

TABLE II
ROVs OF VARIABLES FROM X_2 TO X_5 WITH RESPECT TO X_6

j	$R(X_2)$	$R(X_3)$	$R(X_4)$	$R(X_5)$
2	0.880	0.740	**1.013**	0.909
3	0.697	**1.286**	0.791	1.003
4	0.463	0.627	**1.323**	0.985
5	**1.244**	0.811	0.732	1.032
Total	3.284	3.464	3.859	**3.929**

result indicates that for this pantograph-catenary couple, the dynamic responses related to the structural parameters of the catenary are sensitive under this operation speed. Similarly, the results of PCCF on the right reflect that speeds near 225kmh^{-1} and 215kmh^{-1} are particularly sensitive for the CSWs and non-CSW signal of PCCF, respectively. These results are crucial for inclusion in probabilistic inference such that the influences of speed variation, especially these sensitive speeds, are already considered in the parameter estimation of BN. Consequently, Figure 10 depicts the final clustering results from PHA and PCCF combining those from CSWs and non-CSW signal by applying (19). As the combination between two independent indicators covering different frequency ranges, the percentage of unhealthy condition levels increases compared with the predefined percentile boundaries. Additionally, an overall tendency to increase with the increasing speed is also found in the results of both PHA and PCCF. This result shows that the catenary performance gradually declines as more PIs worsen at higher speeds. This observation is in line with the time-domain PIs extracted from CDS and CDH.

The observations of the final variable SCC X_6 are verified defects quantified through Table I and healthy observations indicated by parent variables. As a variable with incomplete observability, the available observations are assigned to X_6 according to the location of a defect and the corresponding observations of parent variables from X_2 to X_5 that triggered the verifying procedure. In total, 9.090×10^3 observations of defects are assigned to X_6, and 8.446×10^5 healthy observations are found as all values of parent variables are 1, which results in a 55.2% observability of variable X_6. The remainder of the observations and BN parameters are estimated by the EM algorithm such that the BN is finally inferable.

Table II gives the ROVs of variables from X_2 to X_5 when $j \geq 2$ defined by (20). It is shown that at condition

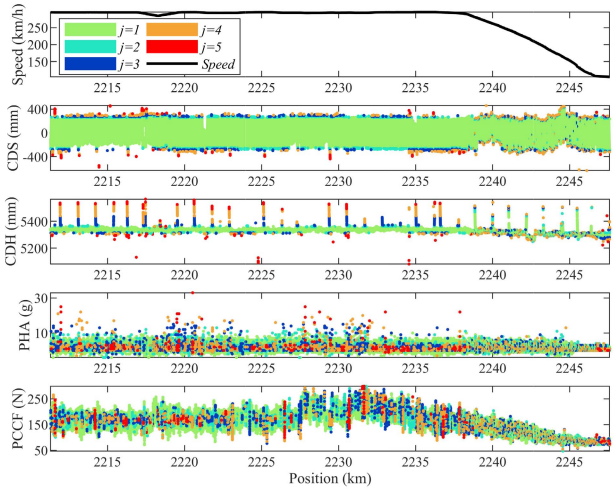

Fig. 11. A segment of new and reconstructed inspection data set with PIs extracted and shown. The speed, CDS, CDH, PHA, and PCCF are depicted from top to bottom.

levels of variable X_6 from 2 to 5, variables representing the PHA, CDH, PHA and CDS have the highest impact on the SCC, respectively. These variables are more indicative at the specific condition level than other variables. Notably, the CDS becomes highly impactful for the worst SCC when $j = 5$, because it is the only source of indicator measured in the lateral direction and thus offers particularly strong evidence indicating a severe condition. Overall, the total ROVs accumulated from all unhealthy SCC show that the PIs of PCCF X_6 contribute the most to an unhealthy SCC among all variables. This observation is in line with the fact that PCCF is considered to be a direct reflection of the catenary performance.

B. Reduction in False Alarms

Hereafter, new inspection data are applied for result analysis. The differences of measurement condition in different inspection runs are considered insignificant for the collection and quality of data. Figure 11 depicts a set of new inspection data for extraction of the BN inputs. The PIs are extracted from the CDS, CDH, PHA and PCCF and are shown by different colors. From the speed profile, it can be observed that this data set represents first a uniform motion followed by a deceleration of the inspection train. The effect of deceleration on the four types of parameters can be observed from 2238 km to the end. The ranges of parameter variation become narrower as the speed decreases. Some unstable vibrations are also found during the deceleration, especially in the lateral direction reflected by the CDS. These effects are considered by the proposed BN with the BN parameters estimated based on historical data with similar characteristics. For the PHA and PCCF, PIs are extracted based on frequency features such that they can indicate an unhealthy condition even when the corresponding time-domain value is low. The speed levels and PIs generated from the new data can be subsequently input into the BN to obtain the output through inference.

TABLE III
IMPROVEMENTS IN HIT RATE AND FALSE ALARM RATE

Type	Amount	Rate	# of SCC $x_6 = j$			Rate of $x_6 \geq 4$
			$j \leq 3$	$j = 4$	$j = 5$	
False alarms	77	0.583	64	10	3	0.169
Hits	55	0.417	2	13	40	0.964

According to the record of on-site verifications performed based on the new segment of inspection data, this data section resulted in a 58.3% rate of false alarm among 132 potential defects verified on site, which is particularly high out of all data sections from the same inspection run. The on-site verification procedures were triggered by predefined thresholds that identified potential defects as peaks or troughs in the data.

By applying the BN-based approach, Table III gives the summarized statistics of the detection results from the data section compared with previous results. The first two columns present the previous results using the traditional threshold-based method that identified 132 potential defects in total. The output KPIs of SCC are the most probable values from BN inference by (22). It can be observed that most of the previous false alarms are recognized as medium risk or lower with $j \leq 3$ and most of the previous hits are recognized as high or extreme risk with $j \geq 4$. When the criterion for determining a potential defect and triggering an on-site verification is that the output risk level at a certain location is high or extreme with a KPI $j \geq 4$, only 16.9% of previous false alarms remain, and 96.4% of previous hits are still correct. This results in an improved false alarm rate of 19.7%, i.e., 66.2% lower than the previous rate, and a new hit rate of 80.3% out of all 66 new potential defects with KPI $j \geq 4$. Both the amount of potential defects and the rate of false alarms are largely reduced according to the output most probable SCC values. Thus, the BN-based approach offers the potential to save a notable amount of maintenance resources if implemented for an entire railway line or network.

As examples, Figure 12 depicts three previous false alarms that are identified as medium or lower risk ($j \leq 3$) by the BN output KPI. In Figure 12(a), the CDH on the top becomes too low, which triggered an on-site verification, while the output KPI using the most probable value (MPV) by (22) and the expected value (EV) by (21) shows that the CDH reflects a medium risk at most, because the PIs of CDH are the only ones indicating unhealthy conditions among all four types of PIs, which lack supporting evidence from PHA and PCCF. Similarly, Figure 12(b) shows a previous false alarm triggered by a sudden rise of PHA in the middle location. However, the PI of PHA is the only indication of an unhealthy condition such that the output MPV and EV are both lower than $j = 4$. The PIs of PCCF in Figure 12(c) suffer from the same lack of supporting evidences, although the time-domain PCCF have high amplitudes and the frequency-domain PIs are $j = 3$.

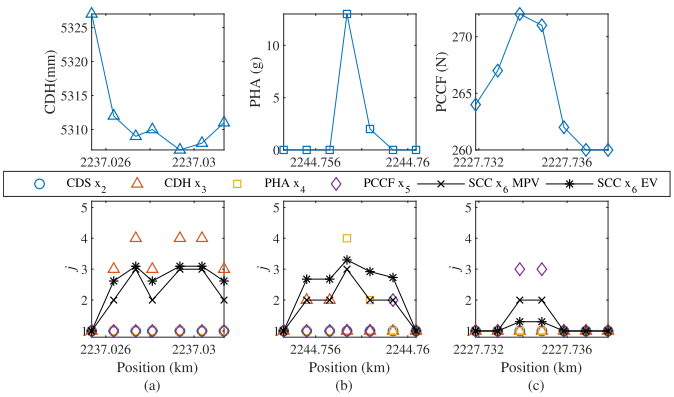

Fig. 12. Three previous false alarms that are identified as medium risk or below ($j \leq 3$) by the BN-based approach. The false alarms were previously triggered by the (a) CDH, (b) PHA and (c) PCCF data shown at the top, respectively. The data PIs and BN outputs using the most probable value (MPV) and the expected value (EV) are shown at the bottom.

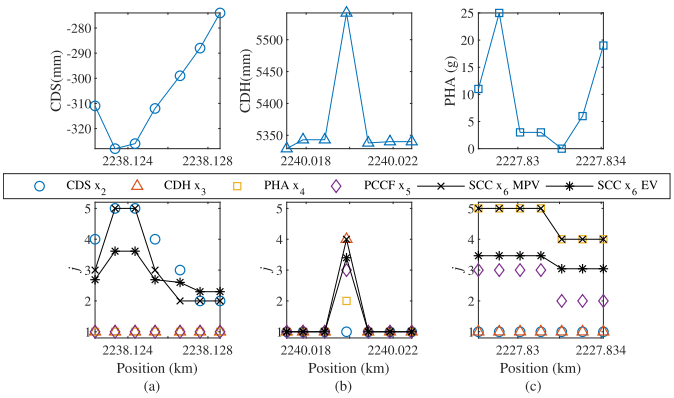

Fig. 13. Three previous hits that are identified as high or extreme risk ($j \geq 4$) by the BN-based approach. The hits were previously triggered by the (a) CDS, (b) CDH and (c) PHA data shown at the top, respectively. The data PIs and BN output KPI using the MPV and the EV are shown at the bottom.

In contrast, Figure 13 shows three examples of previous hits that are also confirmed by the BN-based approach with the output MPV indicating a high or extreme risk. Figure 13(a) shows that an unhealthy PI of CDS is in itself a sufficient indication because it has and requires no supports as the only indicator in the lateral direction. For the unhealthy PIs of CDH and PHA in Figure 13(b) and (c), respectively, they are supported by the unhealthy PIs of PCCF, resulting in high or extreme risks at the corresponding locations. These results also suggest that to confirm whether an on-site verification is necessary, the MPVs should be checked instead of the EVs, which could be smaller than the MPVs due to averaging by probabilities.

Overall, the output of the BN-based approach is effective in reducing the number of potential defects and the false alarm rate. This result is the main merit of the approach that fuses all types of input data into an integrated KPI. Maintenance decisions made based on such a KPI can be more convincing and reliable compared with the current practice.

TABLE IV
RESULTS COMPARISION WITH ALTERNATIVE BN STRUCTURES

BN structure	# of potential defects	False alarm rate
Proposed structure in Figure 2 	66	0.197
Alternative structure 1 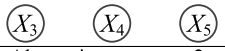	102	0.529
Alternative structure 2 	81	0.370
Original maintenance record	132	0.583

C. Comparison With Alternative BN Structures

The proposed BN structure is crucial for the performance of the BN-based approach. The directed arcs in the structure establish a representation of the physical relations between the included dynamic data types of the catenary. Among all arcs, the two between variables CDH X_3, PHA X_4 and PCCF X_5 are of great importance as correlated dynamic responses in the vertical direction. To show the effects of both arcs, two alternative structures between the three variables are applied to the same data for comparison. As presented in Table IV, alternative structure 1 cancels the arcs between the three variables, and alternative structure 2 reverses the directions of both arcs. The former ignores the physical relations between variables, whereas the latter reverses them.

The alternative BNs are estimated with the same historical data and applied to the new data. The detection results are given in Table IV. Among 132 potential defects from the original maintenance record, all BN structures identify a lower number of potential defects, showing the general effect of combining multiple data types. The proposed structure outputs the least number of potential defects that results in the lowest false alarm rate, and the structure with reverse arcs performs better than the one without any arc. This result is in line with theoretical analysis based on equations from (2) to (6), where the cause-effect relationships are found between the data of CDH, PHA and PCCF in the same manner. Therefore, it is necessary to not only establish the physical relations through arcs, but also set the arc directions in a physics-based manner considering the characteristics of data.

D. Tolerance Against Bad Data

In practice, measurement data can be noisy or missing leading to inaccurate detection results. It is important to address these issues when the detection itself is methodologically difficult to achieve. Although the noisy data can be addressed by denoising techniques using on-board filtering devices or pre-processing procedures before data usage, the randomly missing data are not easy to address. The following discusses variations in the BN outputs based on the same inspection data used above.

1) Noisy Data: The inspection data were pre-processed with high-frequency noises filtered out in all types of measurements except for speed. To test the performance of the BN outputs with general noisy input and the degree of noise tolerance, synthetic noises are added to the inspection data used as a noise-free reference. White noises resulting in a signal-to-noise ratio (SNR) ranging from 0.1dB to 30dB are added to the CDS, CDH, PHA and PCCF data before performing the data reconstruction. A lower SNR means stronger noises that are more likely to contaminate the detection results.

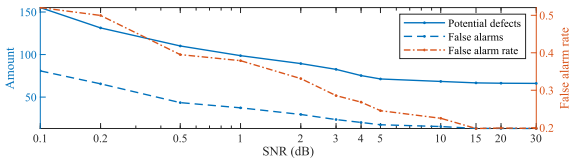

Fig. 14. Detection results when the SNR of input data changes from 0.1dB to 30dB. The left vertical axis show the total amount of potential defects and false alarms while the right one shows the corresponding rate of false alarm.

Figure 14 depicts the detection results using the BN-based approach when the input data contain noises. The statistics under a certain SNR are the average results of generating and adding random noises that satisfy the SNR for ten times. It can be observed that when the SNRs are greater than or equal to 15dB, the results are almost identical to those of the noise-free data that output 66 potential defects and 19.7% false alarm rate. As the SNR decreases, both the amount of potential defects and false alarms increase, leading to increase of the false alarm rate up to 52.1%. Considering that the previous results output by the traditional method have 132 potential defects and a 58.3% false alarm rate, the proposed approach can be acceptable with the false alarm rate limited to below 30% when the SNR is greater than 3dB. This ability to tolerate noise is due to the percentile-based extraction of PIs, which can mitigate the effects of noises. Nevertheless, it is still advisable to pre-process highly noisy data because there are sophisticated methods to improve signal SNRs from below 10dB to higher.

2) Missing Data: Missing data occur commonly and randomly during continuous measurements due to glitches in the measurement system. When only a few sampling points are missing in between recorded data, they can be interpolated based on the adjacent recorded data. However, this process introduces errors into the measurement data that can potentially lead to inaccurate detection results. When a temporary failure of a component in the measurement system occurs during inspections, it causes missing data over a much longer duration, a situation that is not suitable for interpolation. For the inference of the proposed BN, the output KPI can still be estimated if one or more types of input data are missing. In practice, it is unlikely that two or more types of data among the speed, CDS, CDH, PHA and PCCF are missing at the same time because of separately operating sensors and according to historical records. Thus, the performance of the BN-based approach is investigated when one type of missing data are encountered. The missing data are considered to cause the corresponding missing inputs (PIs) for the BN.

a) Short duration of missing data: The randomly missing short-duration data can be neglected unless the event occurs

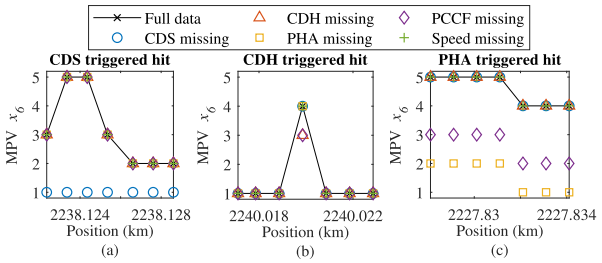

Fig. 15. The output MPVs of three examples of hits when the data is complete and one type of data is missing. The markers falling outside of the solid lines are deviated MPVs caused by the missing of corresponding data.

exactly when the pantograph is passes through a defect of the catenary. In such less likely cases, unhealthy PIs from the missing data are absent for the BN input. For the proposed BN, the missed CDS data are unfavorable because they are the only data measured in the lateral direction that indicate a lateral defect. The missing speed, CDH, PHA and PCCF data are comparatively less impactful, because the speed is not directly linked to the SCC, and the other three types of data are complementary to each other leading to the SCC. Concretely, Figure 15 depicts the output MPVs when one of the five types of data are missing for the three hits shown in Figure 13. Compared with the MPVs from complete data, Figure 15(a) shows that when the defect is reflected by the PI of CDS, only the missing CDS data cause the loss of hit, whereas other missing data minimally influence the output MPVs. In the vertical direction, Figure 15(b) shows that the missing CDH and PCCF data can falsely reduce the output MPVs, when the defect is reflected by the PI of CDH with the PI of PCCF as the main supporting evidence. The upside is that the unhealthy MPVs are not completely eliminated, as in the case missing CDS, which is the sole source of unhealthy PI in the lateral direction. For the same reason, Figure 15(c) shows that when the hit is triggered by the PI of PHA and supported by the PI of PCCF, the loss of PHA and PCCF reduces the MPVs compared with the MPVs from complete data.

b) Long duration of missing data: According to the record of inspection data from the high-speed line studied, this situation has occurred before, i.e., one type of measurement data is almost completely missing due to sudden component failures that could not be instantly fixed on a moving train. It is highly costly to run the inspection again, and thus making use of the incomplete data set is valuable to avoid wasting an inspection run entirely. Using the data shown in Figure 11 as an example, detection results based on the BN output when one of the five types of data is completely missing are obtained. In the case of missing speed, the data partition step (Step 2) in extraction of the BN input must be skipped. Table V presents the number of potential defects and hits identified by the output MPVs when handling long-duration missing data. It can be observed that when a certain type of data is completely missing, it consequently reduces the number of potential defects due to the loss of unhealthy PIs from that type of data. However, the missing CDH, PHA, or PCCF data do not largely reduce

TABLE V
DETECTION RESULTS WHEN ONE TYPE OF DATA IS COMPLETELY MISSING

Data	# of potential defects (MPV $x_6 \geq 4$)	# of hits	Hit rate
Complete	66	53	80.3%
Speed missing	66	52	78.8%
CDS missing	61	48	78.7%
CDH missing	59	50	84.7%
PHA missing	61	51	83.6%
PCCF missing	61	50	82.0%

the number of hits, thus resulting in a higher hit rate at the price of overlooking several potential defects. At the same time, the potential defects overlooked by the missing CDS are all hits that are actually missed, leading to the lowest hit rate. The missing speed data minimally influence the results in this case, because the speed variation of the input data set is rather small. It is expected that the missing speed are more impactful when the speed changes frequently during an inspection.

In the undesired events of missing data, the BN-based approach can still estimate the output KPI of SCC, because it partially extracts and preserves the useful information of the incomplete data set to avoid the total waste of recorded data. Although the outputs are not completely satisfactory in terms of hit rate, especially when the CDS data are missing at defective locations, it is still a manageable situation for the proposed approach, considering that occurrences at the exact locations are few.

VI. CONCLUSION AND OUTLOOK

This study addresses practical problems in condition monitoring of the catenary in high-speed railway lines, including the underutilization of inspection data and the high false alarm rate in defect detection. A generic data-driven approach for improved catenary condition monitoring is proposed. The approach applies a new BN that fuses key information extracted from multiple types of inspection data into a sole KPI. The BN structure is established based on the physical relations between the data of speed, CDS, CDH, PHA and PCCF, which are all crucial data types for assessing the catenary condition. Tailored PIs that can properly reflect the catenary condition are defined and extracted from the CDS, CDH, PHA and PCCF according to their data characteristics resulting from the pantograph-catenary interaction. Using the four tailored PIs as the input of BN, the KPI that indicates the overall catenary condition by considering all input PIs is defined as the BN output. In this way, the KPI can reflect all types of catenary defects causing abnormal dynamic responses in the four types of data. Based on the proposed BN, an approach to obtain the KPI for the comprehensive condition assessment of the catenary is presented.

To test the performance of the BN-based approach, the historical inspection data and maintenance records from a section of the China Beijing-Guangzhou high-speed railway line in the past three years are used as an example. Preliminary results show that with the BN-based approach, the BN outputs

from new inspection data can significantly reduce the false alarm rate by up to 66.2%, thus increasing the hit rate for defect detection. In addition, the effectiveness of the proposed BN is proven by outperforming the alternative BN structures with the same input. Furthermore, the approach is also feasible when the input data quality is poor by acceptably tolerating noisy data with a SNR higher than 3dB or one type of data occasionally missing in inspections.

To further develop the proposed approach, four major improvements can be considered. The first improvement is inclusion of additional data types in the BN structure, such as geometrical data and images, such that the BN output is more comprehensive by covering a wider range of PIs of the catenary. The second one is expansion of the BN output into indicators for specific types of defects such that defect classification can be achieved following detection. The third one is application of automatic feature identification and extraction techniques such as deep learning to define PIs that are beneficial for defect classification. The final one is updating of the BN parameters that consider the different degradation stages in the full service life of the catenary, potentially with a dynamic BN. These improvements require notably large amounts of data and information accumulated from a long-term periodic inspection. To implement this approach for a catenary in practice, it is important to first decide on the monitored data types and thus the BN structure, and the selected measurement data and maintenance records of the catenary should be stored in a manner that is easily traceable through geographic locations or distance marks along the rail.

ACKNOWLEDGMENT

The authors would like to thank the Chinese Academy of Railway Sciences for providing data for this study and the anonymous reviewers for their constructive comments.

REFERENCES

[1] X. Gibert, V. M. Patel, and R. Chellappa, "Deep multitask learning for railway track inspection," *IEEE Trans. Intell. Transp. Syst.*, vol. 18, no. 1, pp. 153–164, Jan. 2017.

[2] M. Molodova, Z. Li, A. Nüñez, and R. Dollevoet, "Automatic detection of squats in railway infrastructure," *IEEE Trans. Intell. Transp. Syst.*, vol. 15, no. 5, pp. 1980–1990, Oct. 2014.

[3] J. S. Lee, S. Choi, S.-S. Kim, C. Park, and Y. G. Kim, "A mixed filtering approach for track condition monitoring using accelerometers on the axle box and bogie," *IEEE Trans. Instrum. Meas.*, vol. 61, no. 3, pp. 749–758, Mar. 2012.

[4] S. Kusumi, T. Fukutani, and K. Nezu, "Diagnosis of overhead contact line based on contact force," *Quart. Rep. RTRI*, vol. 47, no. 1, pp. 39–45, Feb. 2006.

[5] O. Bruno, A. Landi, M. Papi, and L. Sani, "Phototube sensor for monitoring the quality of current collection on overhead electrified railways," *Proc. IMechE F, J. Rail Rapid Transit*, vol. 215, no. 3, pp. 231–241, 2001.

[6] I. Aydin, M. Karakose, and E. Akin, "Anomaly detection using a modified kernel-based tracking in the pantograph–catenary system," *Expert Syst. Appl.*, vol. 42, no. 2, pp. 938–948, Feb. 2015.

[7] J. Leander, A. Andersson, and R. Karoumi, "Monitoring and enhanced fatigue evaluation of a steel railway bridge," *Eng. Struct.*, vol. 32, no. 3, pp. 854–863, 2010.

[8] E. Fridell, M. Ferm, and A. Ekberg, "Emissions of particulate matters from railways—Emission factors and condition monitoring," *Transp. Res. D, Transp. Environ.*, vol. 15, no. 4, pp. 240–245, 2010.

[9] M. Givoni, "Development and impact of the modern high-speed train: A review," *Transp. Rev.*, vol. 26, no. 5, pp. 593–611, Sep. 2006.

[10] A. Collina, F. Fossati, M. Papi, and F. Resta, "Impact of overhead line irregularity on current collection and diagnostics based on the measurement of pantograph dynamics," *Proc. Inst. Mech. Eng. F, J. Rail Rapid Transit*, vol. 221, no. 4, pp. 547–559, Jul. 2007.

[11] *Railway Applications. Current Collection Systems. Technical Criteria for the Interaction Between Pantograph and Overhead Line*, CENELEC, Standard BS EN 50 367, 2012.

[12] *Overall Technical Specifications of High-speed Railway Power Supply Safety Inspection and Monitoring System (6C System)*, Standard 2012.136, Ministry of Railways, China, 2012.

[13] M. Carnevale and A. Collina, "Processing of collector acceleration data for condition-based monitoring of overhead lines," *Proc. Inst. Mech. Eng. F, J. Rail Rapid Transit*, vol. 230, no. 2, pp. 472–485, Feb. 2016.

[14] D. Zhan, D. Jing, M. Wu, D. Zhang, L. Yu, and T. Chen, "An accurate and efficient vision measurement approach for railway catenary geometry parameters," *IEEE Trans. Instrum. Meas.*, vol. 67, no. 12, pp. 2841–2853, Dec. 2018.

[15] P. Boffi *et al.*, "Optical fiber sensors to measure collector performance in the pantograph-catenary interaction," *IEEE Sensors J.*, vol. 9, no. 6, pp. 635–640, Jun. 2009.

[16] E. Karakose, M. T. Gencoglu, M. Karakose, I. Aydin, and E. Akin, "A new experimental approach using image processing-based tracking for an efficient fault diagnosis in pantograph–catenary systems," *IEEE Trans. Ind. Informat.*, vol. 13, no. 2, pp. 635–643, Apr. 2017.

[17] C. J. Cho and H. Ko, "Video-based dynamic stagger measurement of railway overhead power lines using rotation-invariant feature matching," *IEEE Trans. Intell. Transp. Syst.*, vol. 16, no. 3, pp. 1294–1304, Jun. 2015.

[18] S. Bruni, G. Bucca, M. Carnevale, A. Collina, and A. Facchinetti, "Pantograph–catenary interaction: Recent achievements and future research challenges," *Int. J. Rail Transport.*, vol. 6, no. 2, pp. 57–82, 2018.

[19] Z. Liu, Y. Song, Y. Han, H. Wang, J. Zhang, and Z. Han, "Advances of research on high-speed railway catenary," *J. Modern Transp.*, vol. 26, no. 1, pp. 1–23, Mar. 2018.

[20] Z. Liu, L. Wang, C. Li, and Z. Han, "A high-precision loose strands diagnosis approach for isoelectric line in high-speed railway," *IEEE Trans. Ind. Inf.*, vol. 14, no. 3, pp. 1067–1077, Mar. 2017.

[21] J. Chen, Z. Liu, H. Wang, A. Núñez, and Z. Han, "Automatic defect detection of fasteners on the catenary support device using deep convolutional neural network," *IEEE Trans. Instrum. Meas.*, vol. 67, no. 2, pp. 257–269, Feb. 2018.

[22] G. Kang, S. Gao, L. Yu, and D. Zhang, "Deep architecture for high-speed railway insulator surface defect detection: Denoising autoencoder with multitask learning," *IEEE Trans. Instrum. Meas.*, vol. 68, no. 8, pp. 2679–2690, Aug. 2018.

[23] H. Wang *et al.*, "Detection of contact wire irregularities using a quadratic time–frequency representation of the pantograph–catenary contact force," *IEEE Trans. Instrum. Meas.*, vol. 65, no. 6, pp. 1385–1397, Jun. 2016.

[24] Z. Liu, H. Wang, R. Dollevoet, Y. Song, A. Núñez, and J. Zhang, "Ensemble EMD-based automatic extraction of the catenary structure wavelength from the pantograph–catenary contact force," *IEEE Trans. Instrum. Meas.*, vol. 65, no. 10, pp. 2272–2283, Oct. 2016.

[25] H. Wang, A. Núñez, Z. Liu, Y. Song, F. Duan, and R. Dollevoet, "Analysis of the evolvement of contact wire wear irregularity in railway catenary based on historical data," *Veh. Syst. Dyn.*, vol. 56, no. 8, pp. 1207–1232, Dec. 2017.

[26] H. Wang, A. Núñez, Z. Liu, and R. Dollevoet, "Entropy-based local irregularity detection for high-speed railway catenaries with frequent inspections," *IEEE Trans. Instrum. Meas.*, to be published.

[27] R. Zhao, R. Yan, Z. Chen, K. Mao, P. Wang, and R. X. Gao, "Deep learning and its applications to machine health monitoring," *Mech. Syst. Signal Process.*, vol. 115, pp. 213–237, Jan. 2019.

[28] S.-D. Wu, C.-W. Wu, T.-Y. Wu, and C.-C. Wang, "Multi-scale analysis based ball bearing defect diagnostics using mahalanobis distance and support vector machine," *Entropy*, vol. 15, no. 2, pp. 416–433, 2013.

[29] T. W. Rauber, F. de A. Boldt, and F. M. Varejão, "Heterogeneous feature models and feature selection applied to bearing fault diagnosis," *IEEE Trans. Ind. Electron.*, vol. 62, no. 1, pp. 637–646, Jan. 2015.

[30] M. Žvokelj, S. Zupan, and I. Prebil, "Multivariate and multiscale monitoring of large-size low-speed bearings using ensemble empirical mode decomposition method combined with principal component analysis," *Mech. Syst. Signal Process.*, vol. 24, no. 4, pp. 1049–1067, May 2010.

[31] A. Jamshidi *et al.*, "A decision support approach for condition-based maintenance of rails based on big data analysis," *Transp. Res. C, Emerg. Technol.*, vol. 95, pp. 185–206, Oct. 2018.
[32] G. Lederman, S. Chen, J. H. Garrett, J. Kovačević, H. Y. Noh, and J. Bielak, "A data fusion approach for track monitoring from multiple in-service trains," *Mech. Syst. Signal Process.*, vol. 95, pp. 363–379, Oct. 2017.
[33] G. Wang, T. Xu, T. Tang, T. Yuan, and H. Wang, "A Bayesian network model for prediction of weather-related failures in railway turnout systems," *Expert Syst. Appl.*, vol. 69, pp. 247–256, Mar. 2017.
[34] Y. Zhu, H. Limin, and J. Lu, "Bayesian networks-based approach for power systems fault diagnosis," *IEEE Trans. Power Del.*, vol. 21, no. 2, pp. 634–639, Apr. 2006.
[35] F. Sahin, M. Ç. Yavuz, Z. Arnavut, and Ó. Uluyol, "Fault diagnosis for airplane engines using Bayesian networks and distributed particle swarm optimization," *Parallel Comput.*, vol. 33, no. 2, pp. 124–143, 2007.
[36] B. Cai *et al.*, "Multi-source information fusion based fault diagnosis of ground-source heat pump using Bayesian network," *Appl. Energy*, vol. 114, pp. 1–9, Feb. 2014.
[37] N. Friedman, D. Geiger, and M. Goldszmidt, "Bayesian network classifiers," *Mach. Learn.*, vol. 29, no. 2, pp. 131–163, Nov. 1997.
[38] H. Wang, A. Núñez, R. Dollevoet, Z. Liu, and J. Chen, "Intelligent condition monitoring of railway catenary systems: A Bayesian network approach," in *Proc. 25th Int. Symp. Dyn. Vehicles Roads Tracks (IAVSD)*, vol. 2. Rockhampton, QLD, Australia: CRC Press, 2017, Aug. 2017, p. 663.
[39] T. D. Nielsen and F. V. Jensen, *Bayesian Networks and Decision Graphs*. Berlin, Germany: Springer, 2009.
[40] I. Ben-Gal, "Bayesian networks," in *Encyclopedia of Statistics in Quality and Reliability*, vol. 1. Chichester, U.K.: Wiley, 2008.
[41] D. A. Tobon-Mejia, K. Medjaher, and N. Zerhouni, "CNC machine tool's wear diagnostic and prognostic by using dynamic Bayesian networks," *Mech. Syst. Signal Process.*, vol. 28, pp. 167–182, Apr. 2012.
[42] C. Chen, X. Liu, H.-H. Chen, M. Li, and L. Zhao, "A rear-end collision risk evaluation and control scheme using a Bayesian network model," *IEEE Trans. Intell. Transp. Syst.*, vol. 20, no. 1, pp. 264–284, Jan. 2018.
[43] S. Sun, C. Zhang, and G. Yu, "A Bayesian network approach to traffic flow forecasting," *IEEE Trans. Intell. Transp. Syst.*, vol. 7, no. 1, pp. 124–132, Mar. 2006.
[44] N. Friedman, "The Bayesian structural em algorithm," in *Proc. 14th Conf. Uncertainty Artif. Intell.* San Mateo, CA, USA: Morgan Kaufmann, 1998, pp. 129–138.
[45] C. Andrieu, N. De Freitas, A. Doucet, and M. I. Jordan, "An introduction to MCMC for machine learning," *Mach. Learn.*, vol. 50, no. 1, pp. 5–43, Jan. 2003.
[46] *Railway Applications. Current Collection Systems. Requirements for and Validation of Measurements of the Dynamic Interaction Between Pantograph and Overhead Contact Line*, CENELEC Standard BS EN 50317, 2012.
[47] *Railway Applications—Currentcollection Systems—Requirements Forand Validation of Measurements of the Dynamic Interaction Betweenpantograph and Overhead Contact Line*, China National Railway Administration, 2016.
[48] N. E. Huang *et al.*, "The empirical mode decomposition and the Hilbert spectrum for nonlinear and non-stationary time series analysis," *Proc. Royal Soc. London A, Math., Phys. Eng. Sci.*, vol. 454, no. 1971, pp. 903–995, 1998.

Hongrui Wang (S'15) received the B.S. degree in electrical engineering and automation from Mao Yisheng Class, Southwest Jiaotong University, Chengdu, China, in 2012. He is currently pursuing the Ph.D. degree with the Section of Railway Engineering, Delft University of Technology, Delft, The Netherlands.

His research interests include signal processing, machine learning, and their applications in the condition monitoring and maintenance of railway infrastructure.

Alfredo Núñez (M'02–SM'14) received the Ph.D. degree in electrical engineering from the Universidad de Chile, Santiago, Chile, in 2010.

He was a Post-Doctoral Researcher with the Delft Center for Systems and Control, Delft, The Netherlands. Since 2013, he has been with the Section of Railway Engineering, Department of Engineering Structures, Faculty of Civil Engineering and Geosciences, Delft University of Technology. He is currently an Assistant Professor (tenured) in data-based maintenance for railway infrastructure. He was a Work Package Leader with the Development of New Sensor Technologies (static, moving, and crowd-based sensors) for railway networks in Romania, Turkey, and Slovenia, in the European project H2020 NeTIRail-INFRA Project. He has authored a book *Hybrid Predictive Control for Dynamic Transport Problems* in the Series of *Advances in Industrial Control* (Springer-Verlag, 2013). He has coauthored more than 100 international journal papers and international conference papers. He is in the Editorial Board of the Journal *Applied Soft Computing*. His current research interests include the maintenance of railway infrastructures, intelligent conditioning monitoring in railway systems, big data, risk analysis, and optimization.

Zhigang Liu (M'06–SM'16) received the Ph.D. degree in power system and automation from Southwest Jiaotong University, Chengdu, China, in 2003.

He is currently a Full Professor with the School of Electrical Engineering, Southwest Jiaotong University. His current research interests include electrical relationship of vehicle-grid in high-speed railway, power quality considering grid-connect of new energies, pantograph-catenary dynamics, fault detection, status assessment, and active control.

Dr. Liu was elected as a fellow of The Institution of Engineering and Technology (IET) in 2017. He is an Associate Editor of the IEEE TRANSACTIONS ON INSTRUMENTATION AND MEASUREMENT journal. He is also in the Editorial Board of the IEEE TRANSACTIONS ON VEHICULAR TECHNOLOGY journal.

Dongliang Zhang received the B.S. degree in electrical engineering from Southwest Jiaotong University, Chengdu, China, in 2016, where he is currently pursuing the master's degree in electrical engineering. His research interest includes the dynamics and condition monitoring of railway catenary.

Rolf Dollevoet received the M.Sc. degree in mechanical engineering from the Eindhoven University of Technology, Eindhoven, The Netherlands, in 2003, and the Ph.D. degree in rail research on rolling contact fatigue from the University of Twente, Enschede, The Netherlands, in 2010.

Since 2003, he has been with the Railway Sector, ProRail, Utrecht, The Netherlands. Since 2012, he has been appointed as a part-time Professor with the Section of Railway Engineering, Delft University of Technology, Delft, The Netherlands. He was also a Railway System Expert with ProRail, where he was responsible for all the scientific research and innovation with the Civil Engineering Division, ProRail Asset Management.

Dr. Dollevoet was a recipient of the Jan van Stappen Spoorprijs 2010 Award (a yearly prize for contributions to the travel quality and service for passengers in The Netherlands) from the railway sector for his Ph.D. research and its huge potential to reduce track maintenance costs.